Full-scale hybrid fire test in real-time with multiple degree of freedom

Silvio Renard [a,*], Jean-Christophe Mindeguia [b], Fabienne Robert [a], Stéphane Morel [b], Jean-Marc Franssen [c]

[a] Fire Testing Centre, CERIB, Épernon, France
[b] UMR 5295, Institut de Mécanique et d'Ingénierie-Bordeaux (I2M), University of Bordeaux, Bordeaux, F-33000, France
[c] Liege University, Liege, Belgium

Keywords:
Hybrid fire testing
Substructuring

A B S T R A C T

To experimentally assess the fire resistance of civil structures, testing whole structures is very costly but the standard tests on individual structural elements can sometimes be too simplistic, regarding their boundary conditions. Hybrid fire testing offers a promising solution to these limitations, but performing such tests is technically challenging and few full-scale tests have been conducted. Current approaches rely on high-performance sensors and actuator systems, as well as assumptions about the stiffness of the tested element. This paper presents the detailed methodology and results of a full-scale, real-time test with 3 degrees of freedom on a concrete beam. The use of an adaptive controller allowed for maintaining stability and achieving reasonable precision despite the use of relatively low-precision sensors, regular hydraulic actuators, and no assumptions about the tested element's stiffness. The comparison with the same element tested using a standard fire resistance test demonstrates the usefulness of this technique in achieving a more accurate representation of the performance of the tested element in realistic conditions.

1. Introduction

To assess the fire resistance of civil structures, standard fire tests must be carried out when the building elements behaviour under this accidental action is not sufficiently known. Those tests are usually performed on individual building elements, adopting constant mechanical boundary conditions, which may lead to unrealistic results; the behaviour of adjacent structural elements leads to a change in these conditions.

Few tests have been done on entire structures, but the great difficulties of implementation associated with their prohibitive cost make them extremely rare. In this context, the approach known as 'substructuring', or 'hybrid tests', appears as a relevant solution to better take into account the global behaviour of the structure. In hybrid fire tests (HFT), only a part of the total structure is tested experimentally (the so-called "physical substructure", or PS) while the behaviour of the remaining part of the structure is apprehended numerically (the so-called "numerical substructure", or NS).

The first hybrid fire tests have been performed by Korzen et al. [1] on a steel column, with a simplified NS (simply simulated by a constant stiffness value) and with one degree of freedom (DoF) at the interface between the NS and the PS. The same test was later repeated on a concrete column [2].

Robert et al. [3] performed a test with three independently driven jacks for the PS/NS interface, all in the same direction of the axial restrain of a concrete slab.

Mostafaei et al. [4,5] presented a one DoF HFT using an advanced model for the NS, modelled in SAFIR [6], the interaction between the two substructures being manually adjusted.

Whyte et al. [7] developed a thermo-mechanical bench scale single DoF HFT within a framework used in earthquake hybrid simulations. Nontrivial problems were hence exhibited, regarding the interaction between the continuous thermal expansion of the test specimen and the discrete time control, affecting the precision of the tests. Schulthess et al. [8], Tondini et al. [9] and Sauca et al. [10,11] proposed new algorithms dedicated to HFT, as the previously used ones were found to be conditionally stable. These methodologies use strong assumptions on the PS properties such as its tangent stiffness.

Qureshi [12] proposed a methodology to update the stiffness used by the algorithm during the test, based on the initial tangent stiffness and the measurements performed during the test to increase the stability of the test.

Mergny et al. [13] developed an improved test methodology adapting control theory in the form of a PI control loop. This allowed to drastically reduce the errors due to the delays present in the previous

* Corresponding author.
E-mail address: s.renard@cerib.com (S. Renard).

https://doi.org/10.1016/j.firesaf.2024.104233

methodologies and obtained a good precision with the use of an initial tangent stiffness. Another approach, using continuous command and extrapolation is developed by [14] and applied with success to a full-scale one DoF HFT of a steel column.

Schulthess et al. [15] showed that an update of the tangent stiffness during the test increases precision of the test but is challenging in the case of multiple DoF HFT.

Mergny *et al.*[16] performed a successful experimental validation of the PI control methodology on a medium scale with one, two and three DoF HFT of steel columns.

A new methodology enabling the control system to fully mimics the dynamical behaviour of the NS is developed by Qureshi et al. [17], allowing tests to be carried out without any hypothesis on the PS, at the cost of using simplified NS and high performance sensors, controls and actuators.

Finally, Sauca et al. [18] presented an experimental verification of a new algorithm based on dynamic relaxation, introduced by Abbiati et al. [19], adding fictitious masses and damping to the system in order to ensure stability.

The two main limiting factors identified from this literature survey are (i) the need for a precise estimation of the PS stiffness to ensure the stability and accuracy of the control algorithm and (ii) the need of high-performance sensors, control system and actuators to prevent unacceptable force oscillations on stiff PS. To tackle the first problem, the practice is to choose a conservative value for the PS stiffness alongside with an algorithm that remains stable when this stiffness degrades as this is expected during the fire test. The second problem can be addressed by the use of screw actuators for bench scale tests to prevent oscillation, the use of very high precision displacement transducers like LVDTs and fast actuator controller with an interpolation/extrapolation procedure to prevent the ramp and hold behaviour between time steps. Hybrid fire tests are still at the research stage today and there is no reliable and efficient method for carrying them out in the context of a fire resistance study.

In a previous publication [20], the authors present a methodology using a new control procedure associated with a dedicated adaptive controller to overcome those drawbacks. Indeed, it enabled the use of hydraulic actuators with low precision displacement transducers and slow actuator controller. Furthermore, no estimation of the PS stiffness is needed. This methodology had only been validated by pure numerical simulation and a simplistic bench scale test. The present paper demonstrate the effectiveness of this testing procedure through a full-scale, real-time, multiple-degree-of-freedom hybrid fire test performed on a reinforced concrete beam at the Fire Testing Center laboratory located in Épernon, France.

2. Testing procedure and controller

The challenge of a hybrid fire testing procedure is to simultaneously maintain displacement compatibility and to keep force equilibrium errors between the substructures as low as possible during the test, hence to satisfy:

$$\begin{cases} \mathbf{u}_{PS} = \mathbf{u}_{NS} \\ \mathbf{f}_{PS} = -\mathbf{f}_{NS} \end{cases}$$

with $\mathbf{u}_{PS}$ and $\mathbf{u}_{NS}$ the position of the PS and NS at the interface respectively and $\mathbf{f}_{PS}$ and $\mathbf{f}_{NS}$ the forces at the interface of the PS and NS.

As mentioned above, the first anticipated problems are the direct displacement feedback control in the case of stiff structures and the unknown tangent stiffness of the tested specimen. A specific testing procedure was developed to avoid both.

First, the direct displacement feedback control was prevented by implementing a procedure that employs non-equilibrium forces feedback. This procedure, illustrated in Fig. 1 directly imposes the compatibility

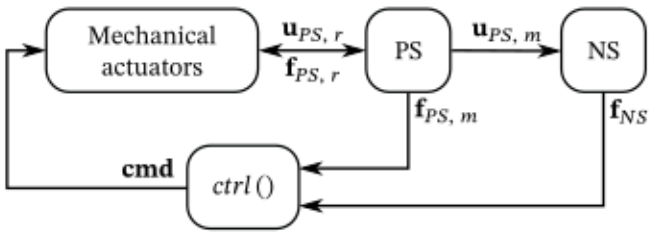

Fig. 1. Non equilibrium forces feedback procedure. The subscript 'm' denotes a measured value and 'r' denotes a real one, without any measurement error.

Table 1
Parameters used for the adaptive controller.

Parameter	Value	Note
c	0.3	Target minimal convergence speed
$\mathbf{p}_0$	$\mathbf{I} \cdot 10^{-6}$	Adaptive gain initial value
a	1.3	Learning gain
T_{max}	5	Period in time steps of oscillation considered as quick
$\mathbf{f}_{min}$	[1000, 1000, 1339]	Smallest significant force (*N*): $\max\left(\mathbf{K}^*_{NS} \times \left(\Delta^*_{\mathbf{u}}\right), \Delta^*_{\mathbf{f}}\right)$.
$\Delta\mathbf{v}_{min}$	$1 \cdot 10^{-5}$	Smallest significant control increment

as the interface displacement of the NS $\mathbf{u}_{NS}$ with the measured displacements of the PS $\mathbf{u}_{PS,m}$, setting $\mathbf{u}_{NS} = \mathbf{u}_{PS,m}$. A properly chosen function *ctrl*() calculates the value of the mechanical actuators input command **cmd** based on $\mathbf{f}_{NS}$ and $\mathbf{f}_{PS,m}$ the measured forces at the interface of the PS.

Then, an adaptive controller is chosen for the function *ctrl*(), designed to enable good performances of the control with a limited number of hypotheses:

- all the dynamic interactions are neglected;
- the sum of the tangent stiffness of the substructures interface $\mathbf{K}_{PS} + \mathbf{K}_{NS}$ is strictly diagonally dominant and slowly varying over the control procedure time step;
- the signs of these diagonal terms are known;
- the actuator system relative degrees for large input command and their signs against the displacements are known.

In the present case, all these conditions are considered to be satisfied, and the relative degree is defined at 1. The relative degree being the number of successive time deviates one have to perform on the controlled variables for the control variables to appear explicitly. Here the controlled variables are a function of the position and the control variables are the spools positions of the control valves of the hydraulic jacks. Hence, neglecting the leakage and with a sufficiently large valve opening, the controlled jack speed is a function of this value. In other words the input command of the actuator will be a function of the first derivative of the displacements, hence the speed of the jacks.

The adaptive controller, inspired by sliding mode control [21], is based on the hypothesis that the DoF can be processed independently according to the algorithm 1. It uses a set of predefined constants given in Table 1. One can note that no parameter depends on measured or assumed properties of the PS, which is a clear advantage in the perspective of a hybrid fire test. The first four parameters have been found to provide good results on various simulated and real tests cases. The last two parameters are based on hypotheses on the expected stiffness of the NS during the test $\mathbf{K}^*_{NS}$ and precision of the measurement system $\Delta^*_{\mathbf{u}}$ and $\Delta^*_{\mathbf{f}}$. The testing procedure is described in detail in the authors previous publication [20]. It is summarised hereafter.

Algorithm 1 *ctrl*() function, the adaptive controller. The indice ^{i} denote the actual time-step. The symbols & and | indicate AND and OR logical operations.

Update variables:

$f^i = f^i_{PS,m} + f^i_{NS}$

$\dot{f}^i = f^i - f^{i-1}$

$\sigma^i = c \cdot f^i + \dot{f}^i$

Qualify the system behaviour:

$q^i_{sm} = \text{sign}\left(\sigma^i\right) \neq \text{sign}\left(\sigma^{i-1}\right)$ → *the sliding surface is crossed*

$q^i_{osc} = \left|\text{atan2}\left(f^i, \dot{f}^i\right) - \text{atan2}\left(f^{i-1}, \dot{f}^{i-1}\right)\right| > \pi / T_{max}$ → *trajectory compatible with quick oscillations*

$q^i_{prec} = \left(\frac{f^i}{f_{min}}\right)^2 + \left(\frac{\dot{f}^i}{f_{min}}\right)^2 < 1$ → *system is considered to have converged*

$q^i_{dir} = \text{sign}\left(\frac{c}{c+1} \cdot f^i + \dot{f}^i\right) \neq \text{sign}\left(\sigma^i\right)$ → *excessive control effort could pull the system trajectory away from the sliding surface*

$q^i_{inc,tmp} = \sim \left(q^i_{prec}\ \&\ q^i_{sm}\ \&\ q^i_{osc}\ \&\ q^i_{dir}\right)$

$q^i_{inc} = q^i_{inc,tmp}\ \&\ q^{i-1}_{inc,tmp}$ → *the control gain should increase*

$q^i_{dec} = \sim q^i_{prec}\ \&\ \left(q^i_{sm} | q^i_{osc}\right)$ → *the control gain should decrease*

Update the gain:

if $\left(q^i_{inc}\right)$ **:**

  $p^i = p^{i-1} \cdot a$

if $\left(q^i_{dec}\right)$ **:**

  $p^i = p^{i-1} / a$

Validate the new gain and update the cmd output:

$\Delta v^i = p^i \cdot \left(\frac{c}{c+1} \cdot f^i + \dot{f}^i\right)$

if $\left(\Delta v^i < \Delta v_{min}\ \&\ p^i < p^{i-1}\right)$ **:** → *variation considered too small, gain not decreased*

  $p^i = p^{i-1}$

  $\Delta v^i = p^i \cdot \left(\frac{c}{c+1} \cdot f^i + \dot{f}^i\right)$

$cmd^i = cmd^{i-1} + \Delta v^i$

if $\left(cmd^i > cmd_{max}\right)$ **:** → *the output command is outside the admissible values*

  $cmd^i = cmd_{max}$

  $p^i = p^{i-1}$

if $\left(cmd^i < cmd_{min}\right)$ **:**

  $cmd^i = cmd_{min}$

  $p^i = p^{i-1}$

3. Case study

3.1. Reference structure and fire scenario

The tested structure is a 3-storey reinforced concrete building prototype, considered as a 2D moment resisting frame, directly inspired from the works of Sauca et al. [22] and illustrated in Fig. 2. The beams spans are 5.6 m long in the main frame axis and the storey height is 3 m. The beams have a 40×25 cm^2 cross section with concrete cover on the longitudinal bars of 40 mm horizontally and 30 mm vertically, see 3. The concrete columns have a 40×40 cm^2 cross section, reinforced with 8 longitudinal rebars with a diameter of 16 mm and a nominal cover of 35 mm. The 47 MPa compressive strength concrete is reinforced with cold worked class B grade 500 steel. The applied loads are summarised in Figs. 4 and 5. The particular representation of the load on the heated beam is dictated by the fact that this represents the disposition of hydraulic jacks on the PS in order to induce in the PS a similar bending moment as if the beam would be subjected to a uniformly distributed load. The same disposition is thus applied on the frame when analysed as a whole to make meaningful comparisons.

The fire takes place in the second compartment of the last floor. The surfaces depicted in red in Fig. 2 will be exposed to an ISO 834-1 fire curve [23] (measured with plate thermometers for the PS). This includes 3 faces of the beam and one face plus 10 cm on each lateral

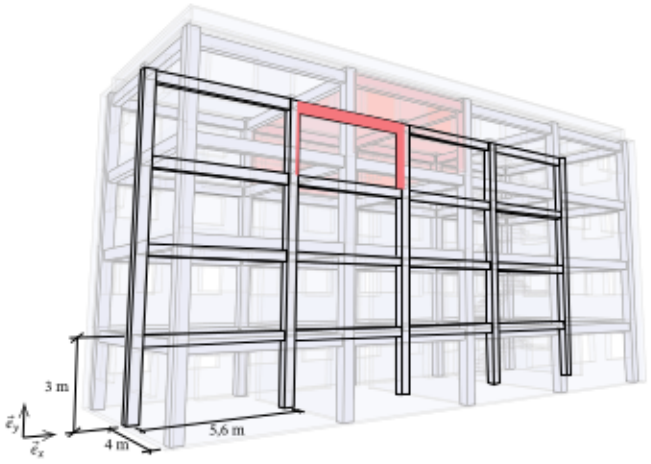

Fig. 2. Global 3D view of the reference structure, the fire compartment and the 2D studied frame.

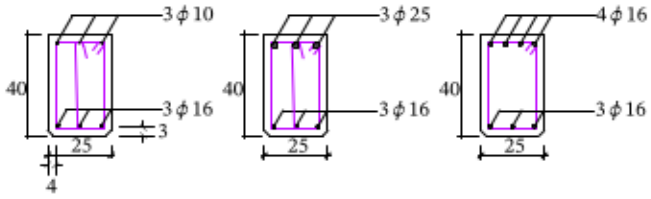

Fig. 3. Beams cross sections, at mid span, near the intermediate supports and near the peripheral supports respectively.

Fig. 4. Distributed loads applied to the 2D frame, the physical substructure is depicted in red. (For interpretation of the references to colour in this figure legend, the reader is referred to the web version of this article.)

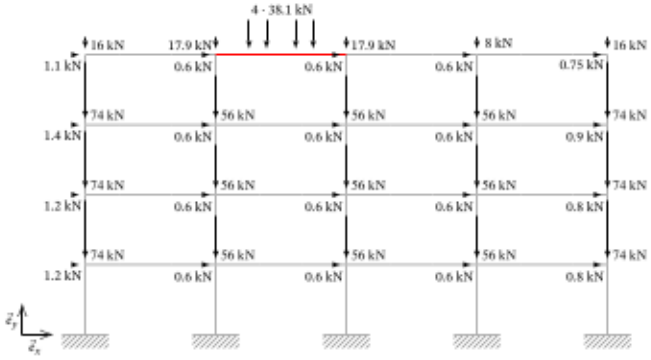

Fig. 5. Point loads applied to the 2D frame, the physical substructure is depicted in red. (For interpretation of the references to colour in this figure legend, the reader is referred to the web version of this article.)

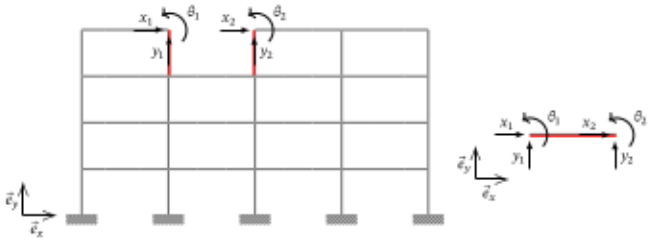

Fig. 6. Initial sub-structured problem with 6 degrees of freedom. On the left the NS, on the right the PS. The parts in red are exposed to ISO 834-1 fire curve. (For interpretation of the references to colour in this figure legend, the reader is referred to the web version of this article.)

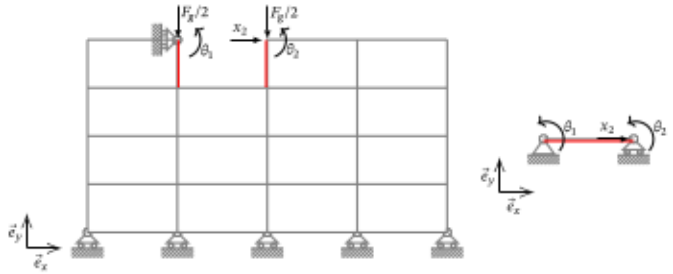

Fig. 7. Simplified system with 3 degrees of freedom. On the left the NS, on the right the PS. The parts in red are exposed to ISO 834-1 fire curve. (For interpretation of the references to colour in this figure legend, the reader is referred to the web version of this article.)

side for the two columns to take into account the presence of the compartmentation walls.

3.2. Sub-structuring and simulation

The reference structure is divided in two sub-structures: the tested element (PS) will be the fire exposed beam and the remaining of the structure (NS) will be simulated with fibre beam finite elements. The interface between the PS and the NS is hence composed by both beam extremities. With the hypothesis of a 2D behaviour for the moment resisting frame, this results in a 6 degrees of freedom system (3 for each point), see Fig. 6. $\mathbf{u}$ is the displacement vector and $\mathbf{f}$ the corresponding reaction forces vector:

$$\mathbf{u} = \begin{bmatrix} x_1 \\ y_1 \\ \theta_1 \\ x_2 \\ y_2 \\ \theta_2 \end{bmatrix} ; \mathbf{f} = \begin{bmatrix} F_{x,1} \\ F_{y,1} \\ M_1 \\ F_{x,2} \\ F_{y,2} \\ M_2 \end{bmatrix}$$

It would yet be quite challenging in an experimental setup to control the 6 degrees of freedom at the interface of the beam by 6 actuators, acting simultaneously with the actuators that apply the load in the span. It is preferable to eliminate the three rigid body modes of the PS from the problem. A more detailed methodology is described in [24] and its application to the present case is summarised hereafter.

Without loss of generality, the usual corotational transformations are not directly applicable here because external forces are applied to the PS outside its extremities nodes. However, as these external forces are gravity loads, this problem is translation-invariant. Furthermore, the rotations is expected to be negligible.

The following hypotheses are then made:

1. The differential vertical displacement between both sides of the beam is neglected on the side of the NS so $y_1 = y_2$, then the gravity loads of the PS F_g are equally distributed on each extremity during the whole test.
2. The shear force due to the difference between the bending moments at each sides of the beam is neglected in front of the shear forces dues to the loads; $\frac{\|M_1+M_2\|}{l} \ll F_g$, in other words, the vertical forces between the beam extremities and the columns do not depend on the moments and are kept constant and equal:

$$F_{y,1} = F_{y,2} = -F_g/2$$

With a reformulation of the initial problem and considering these hypotheses, the resulting system has only 3 active DoF as depicted in Fig. 7.

Two so called 'passive' DoF are defined to take into account the vertical forces between the PS and the NS. They are called 'passive' because there is by hypothesis only a single way coupling between the two sub-structures along these directions.

$$\mathbf{u}_{\text{passive}} = \begin{bmatrix} y_1 \\ y_2 \end{bmatrix} ; \mathbf{f}_{\text{passive}} = \begin{bmatrix} -F_g/2 \\ -F_g/2 \end{bmatrix}$$

Hence, $\mathbf{u}_{\text{passive}}$ will be relaxed as a DoF, not imposed anywhere becoming a result of the simulation and $\mathbf{f}_{\text{passive}}$ will be imposed on the side of the NS.

The displacement and reaction force vectors are hence simplified to:

$$\mathbf{u} = \begin{bmatrix} x_2 \\ \theta_1 \\ \theta_2 \end{bmatrix} \mathbf{f} = \begin{bmatrix} F_{x,2} \\ M_1 \\ M_2 \end{bmatrix}$$

The simulation of the NS is performed by the finite element software SAFIR [6]. The mechanical parameters of the materials are corresponding to siliceous aggregate concrete with a 47 MPa compressive strength and reinforcement in cold worked class B grade 500 steel, and a Young modulus of 200 GPa. The material law used are the one depicted in the Eurocode 2 [25]. The Eurocode 1 [26] heat transfer parameters are also used, with a convective coefficient $h_{fe} = 25\ \text{W} \cdot \text{m}^{-2} \cdot \text{K}^{-1}$ on the exposed surfaces, and $h_{fne} = 4\ \text{W} \cdot \text{m}^{-2} \cdot \text{K}^{-1}$ on unexposed ones. The volumetric mass density of the concrete is defined at $2300\ \text{kg} \cdot \text{m}^{-3}$, its water content to 1.5% and its thermal conductivity is defined from the mixed curve from the Eurocode 2.

Prior to carry out the hybrid fire test, the global behaviour of the whole structure has been simulated by SAFIR. The mechanical results have then been compared to a 'numerical' sub-structuration of the structure, with the 3 DoF defined in Fig. 7. In that case the behaviour of the PS is numerically simulated by SAFIR. Negligible differences were observed between both numerical simulations, proving the reliability of the DoF simplification.

4. Experimental setup

The experiment was carried out with the 'Promethee' facility at the CERIB Fire Testing Centre (France). It consists in a modular fire resistance furnace (up to 6 m × 4 m of horizontal fire exposure and up to 6 m high vertical fire exposure) surrounded by a modular loading structure.

4.1. Actuation system and forces measurement

The aim of the actuation system is to impose variations of x_2, θ_1 and θ_2 values according to the control algorithm command and provide the external loading to the physical substructure as illustrated in Fig. 8. The beam rest on rolling supports, with a horizontal stop on one end. A hydraulic jack on the other end induces variation of x_2. The jack and the stop are both mounted on vertical low friction ball linear guides and equipped with a passive weight compensating jack. For θ_1 and θ_2, lever arms are added at each end of the beam, to allow vertical hydraulic

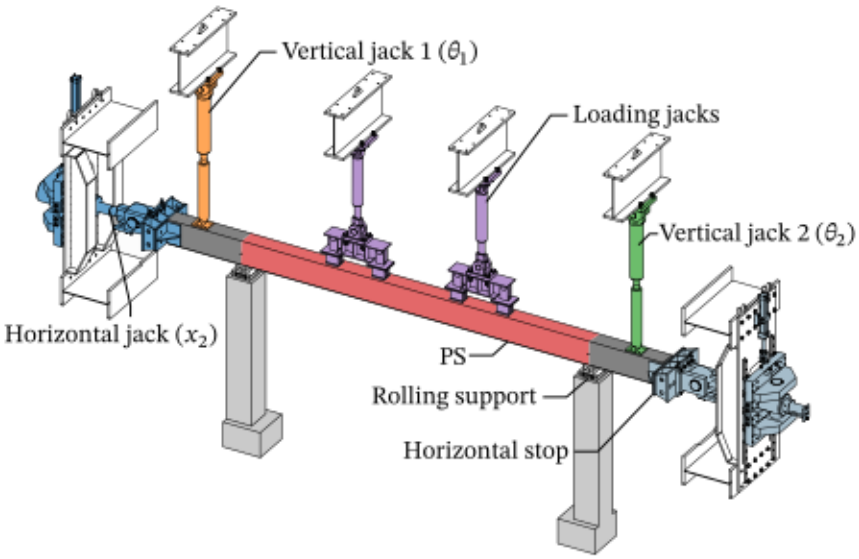

Fig. 8. Actuation system and physical substructure.

jacks to induce rotations on the supports of the beam. The loading of the span is ensured by two hydraulic jacks.

As implemented, the corresponding forces responses $F_{x,2}$, M_1 and M_2 are retrieved by pressure measurements in the chambers of the hydraulic jacks. The expected error of these measurements will be taken as $\Delta_f^* = 1000$ N for the setup of the adaptive controller.

All the jacks except the weight compensating ones are controlled via direct drive servo-valves. These valves take as input command a desired position for their spools. For the loading jacks, these spools positions set points are controlled by a classic force feedback PID regulation. For the others, the spools positions set points are directly controlled by the output of the adaptive controller.

4.2. Displacement measurement

Due to the expected efforts and the potential thermal effects (support deformations), no points on the loading structure or the supports can be considered fixed. Hence, all the displacements are measured from an independent supporting structure illustrated in Fig. 9, assuming that the deformations of the laboratory strong floor are negligible.

The vertical and horizontal displacements of both ends of the PS Δx_1, Δy_1, Δx_2 and Δy_2, are deduced via the measurements of 8 wire position sensors. These sensors are measuring their relative distance to 4 measurement points: two wire position sensors placed to roughly form a right angle for each points as illustrated by the detail view of Fig. 9. Hence, the displacement of one end of the PS is calculated as the mean of the displacements of two measurement points situated on both lateral sides of the beam at mid height. Then, with the hypotheses of an initial length of 5.6 m and a zero initial inclination, triangulation calculations are performed (not further described in the context of this publication, details can be found in [24]), to deduce:

- the actual length of the beam and hence the value of x_2 to be imposed to the NS;
- φ_m the rigid body rotation of the beam.

Two inclinometers are placed on the top of the beam, measuring the variation of their inclination $\Delta\varphi_1$ and $\Delta\varphi_2$. These values, combined to φ_m allows calculating θ_1 and θ_2 in order to be imposed to the NS. The expected error of these measurement for the design of the controller is $\Delta_{x_2}^* = 40$ µm and $\Delta_{\theta_1}^* = \Delta_{\theta_2}^* = 18$ µrad which are the quantisation step of the sensors.

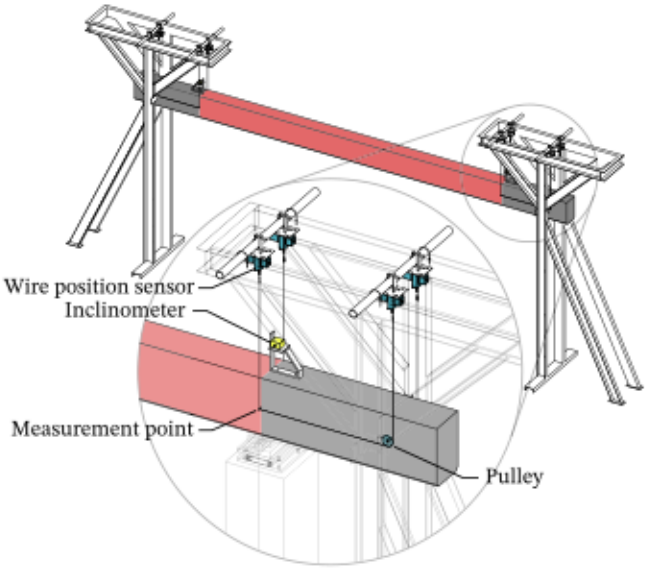

Fig. 9. Displacement measurement setup. The red part of the beam is the PS in this study. (For interpretation of the references to colour in this figure legend, the reader is referred to the web version of this article.)

4.3. Physical specimen and implementation

The physical specimen is an 8 m long reinforced concrete beam of which the 5.6 m central part is the actual PS. The heavily reinforced extremities are used for the actuation and force measurement. The beam is instrumented with 32 thermocouples installed before the casting. This specimen has been done in the context of the work of [22] about four years before the presented test. It has been stored at around 23 ° C and 40 % of relative humidity. The concrete compressive strength has been measured at 48 MPa (mean value of three cylinder tests). The water content has been measured on two representative 25 cm cylinders sealed in a water tight foil except for its extremities, at around 1.4 % near the surface and 2.5 % at the centre of the section.

This specimen is installed in the horizontal furnace as illustrated in Figs. 10 and 11. The displacement measurement wires are protected

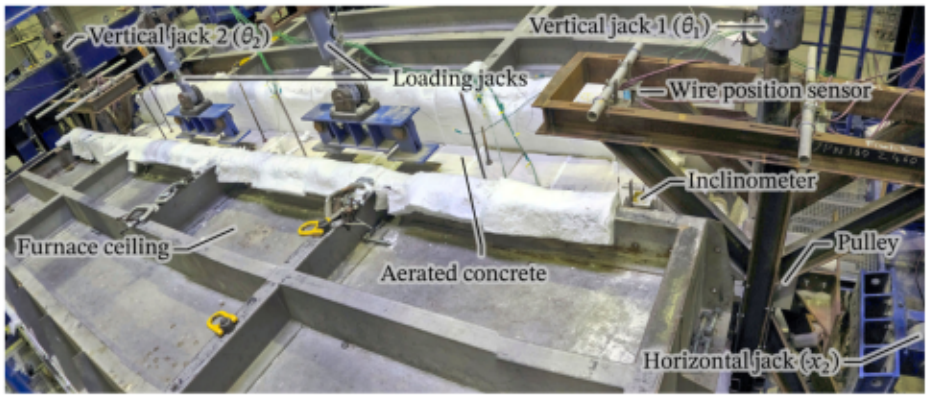

Fig. 10. Top view of the experimental setup.

with casing fixed to the beam. The rolling supports and columns are insulated with mineral wool. Twelve plate thermometers are installed around the beam to control the furnace burners.

5. Results

5.1. Start of the test

The test is performed in three phases, the contact phase, the mechanical loading of the structure at ambient temperature (*i.e.* the constant vertical point forces at the beam span) and then the fire test.

In the first phase, all the actuators are driven by force feedback control and brought into contact with the PS with small forces set points (< 500 N). The interface actuators are already driven by the adaptive controller, replacing $\mathbf{f}_{NS}$ by force set points. When the actuators are in contact, all the displacements are set to 0 and the NS simulation start. At the same moment, the control of the three interface actuators is switched from the force feedback control to the non equilibrium force feedback procedure. From this point, the two substructures are supposed to be kept compatible and at equilibrium by the HFT procedure until the end of the test. Then the two substructures are simultaneously loaded using a linear ramp of 1200 s. Three repetition of the loading phase are performed but only the last one is shown in the data. Then, after a stabilisation phase of 1000 s, the gas burners of the furnace is turned on, alongside with the beginning of the simulated thermal loading of the NS.

5.2. Temperature measurements and observations during the test

The time $t = 0$ is defined as the moment when the mean temperature measured by the 12 plate thermocouples reaches 45 ° C. The gas burners are automatically controlled to follow the EN 1363-1 prescriptions (*i.e.* the ISO 834-1 fire curve), based on plate thermocouples measurements. The temperature of the plate thermocouples as well as the error and tolerances are presented in Fig. 12.

During the test, endoscopic cameras enabled the observation of spalling in the central part of the span at one of the lower corners of the beam at $t = 1387$ s. The same phenomenon was observed on the second lower corner, at $t = 1527$ s. These phenomena explain the large discrepancy between the predicted (thermal simulation done with SAFIR) and measured temperature for the lower corner rebars shown in Fig. 13.

The failure of the beam is observed at $t = 9880$ s after a sudden acceleration of the measured deflection, with a sudden drop of M_1, followed by M_2 a few seconds after. The mode of failure of the beam is further analysed in Section 5.5.

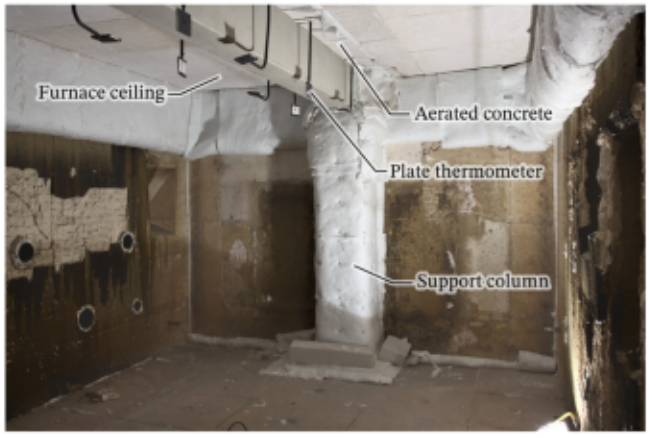

Fig. 11. Bottom view of the experimental setup.

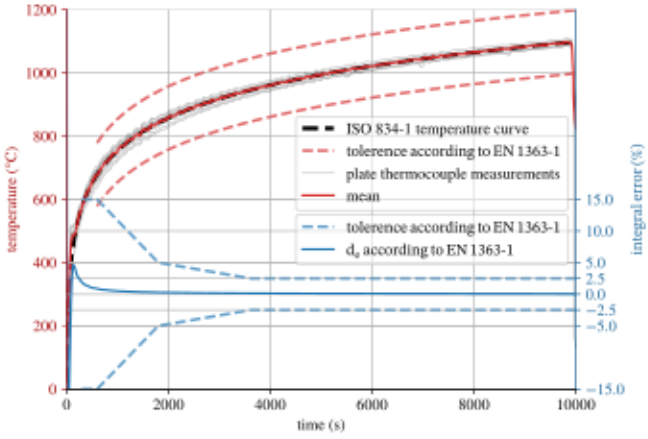

Fig. 12. Temperatures measured by the plate thermometers during the test and prescriptions of the EN 1363-1.

5.3. Interface displacements and forces

The interface positions during the test are presented in Fig. 14. The measured and calculated forces at the interface are reported in Fig. 15.

At $t = -2200$, all the displacements are set to 0 and the NS simulation start. At this point, both substructures are then mechanically compatible and at equilibrium. During the following 1200 s ($-2200 < t \leq 1000$), the structures are loaded. The sub-structures are kept loaded

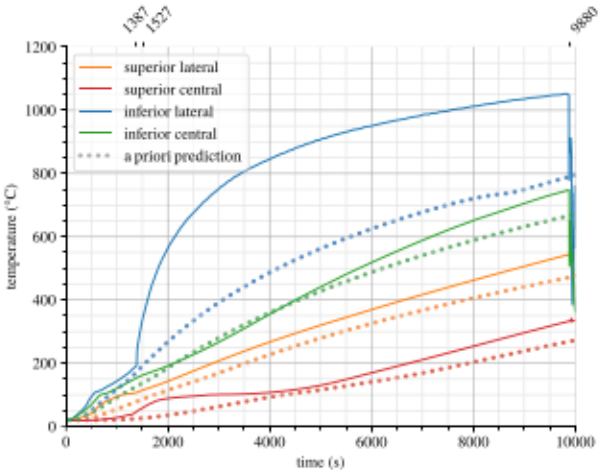

Fig. 13. Measured temperatures of the longitudinal rebars and comparison with the a priori simulation done with SAFIR.

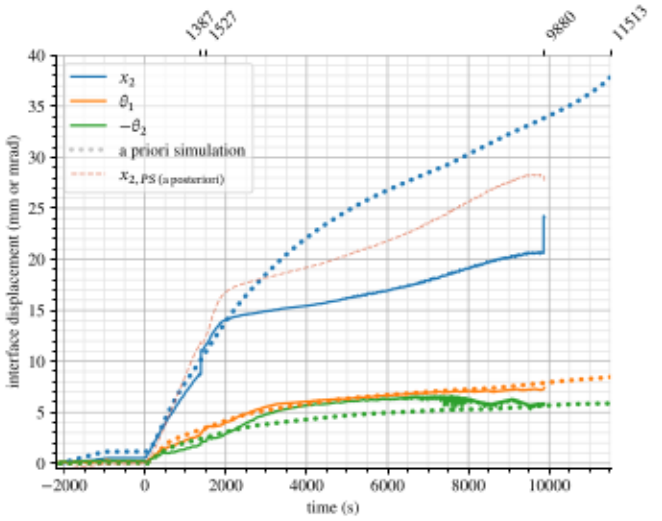

Fig. 14. Measured displacements on the substructures' interface and comparison with the a priori simulation of the whole structure with SAFIR.

and at equilibrium and compatibility during 1000 s ($-1000 < t < 0$) and then the fire test starts at $t = 0$.

At the beginning of the fire test, the temperatures increase and the thermal gradients in the structure elements induce a modification of their equilibrium position. The thermal gradient effect on the beam alone would lead a negative value for the rotation θ_1 and a positive value for θ_2 while the reverse stands for the columns on the side of the NS. In this hybrid test, the interface displacement shows that the dominant elements are the columns as a positive rotation of θ_1 and a negative rotation of θ_2 are observed. This phenomenon leads to a fast increase of the interface moments M_1 and M_2. The thermal gradient in the heated columns on the side of the NS would induce an increase of x_2 and a decrease of $F_{x,2}$. However, the mean thermal expansion of the beam induce an increase of both x_2 and $F_{x,2}$. After $t = 1900$ s, the materials thermal degradation and hence the reduction of the second moment of area lead to a decrease of the bending moments while the thermal expansion of the beam still induces an increase of x_2 and $F_{x,2}$.

At the time of the first spalling, $t = 1387$ s, a sudden increase of the measured length is observed. At the very same time, a decrease of $F_{x,2}$ is measured which is not a consistent behaviour. Another unexplained sudden increase occurs at $t = 9965$ s. After further investigation, these sudden variations are measured by only one of the position sensors, suggesting a malfunction of the sensor. A *a posteriori* calculated value of $x_{2,PS}$ excluding the malfunctioning sensor is illustrated on Fig. 14, showing a large error on the compatibility between the two substructures due to this sensor failure. Nevertheless, the influence of this large error on the measured displacements must be put in perspective with the low relative stiffness of the NS in this direction.

5.4. Performance of the HFT procedure and controller

As the compatibility is directly imposed between the two substructures, the performance metric will be a relative error calculated as:

$$errF_{x,2,PS} = \frac{F_{x,2,PS} + F_{x,2,NS}}{|F_{x,2,PS}|}$$

and similarly, for $errM_1$ and $errM_2$.

These errors, illustrated in Fig. 16 are below 10% during nearly all the test; the HFT procedure and controller exhibit a good behaviour, even in the presence of the large displacement leaps previously discussed.

As expected, the procedure associated with the adaptive controller behaves well on the stiff axial degree of freedom even with limited precision transducers and hydraulic actuators. Indeed, with a displacement

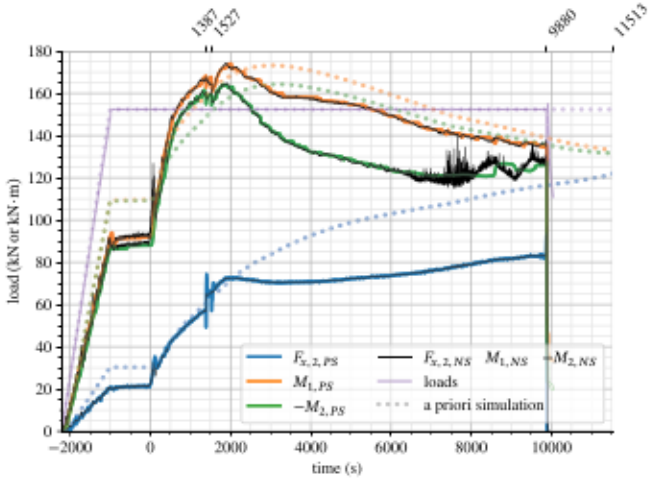

Fig. 15. Measured loads and forces at the interface of the substructures and comparison with the a priori simulation of the whole structure with SAFIR. The coloured continuous lines represent the measured values of the forces on the side of the PS. The continuous thin black lines are the values on the side of the NS. (For interpretation of the references to colour in this figure legend, the reader is referred to the web version of this article.)

feedback control loop, an oscillation between two quantisation steps $\Delta^*_{x_2} = 40$ µm is expected in the best case, leading, with an estimated axial stiffness of 479 MN·m^{-1}, to more than 180 % relative error during the phase at ambient temperature, compared to less than 3 % with the presented methodology.

As also expected, the advantage of this methodology vanishes in the case of soft degree of freedom. Again, an oscillation between two quantisation steps $\Delta^*_{\theta} = 18$ µrad leads, with an estimated stiffness of 25.6 MN · m · rad^{-1} to around 1 % of relative error in the best case, comparable with the observed 2 %.

On the rotational degree of freedom, low frequency oscillations are observed, and the precision is not optimal. This behaviour has been observed in fully numerical simulations of HFT and associated with an underestimation of the expected precision of the transducers. Indeed, the value of $\Delta^*_{\theta} = 18$ µrad seems overly optimistic and based on tests made on the transducer alone excluding the possible increase of the measurement noise likely created by the increased working temperature and the functioning furnace. In this case, the adaptive gain is overly reduced, interpreting the noise as real oscillations as

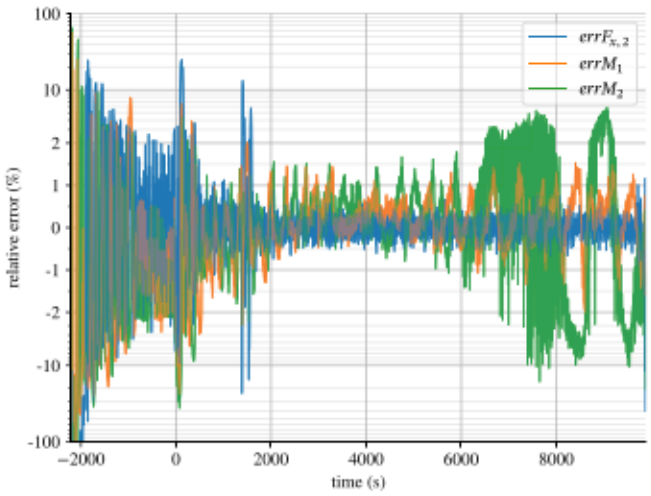

Fig. 16. Relative equilibrium errors between the forces at the interface of the two substructures during the test. The ±2 % vertical scale is linear and logarithmic elsewhere.

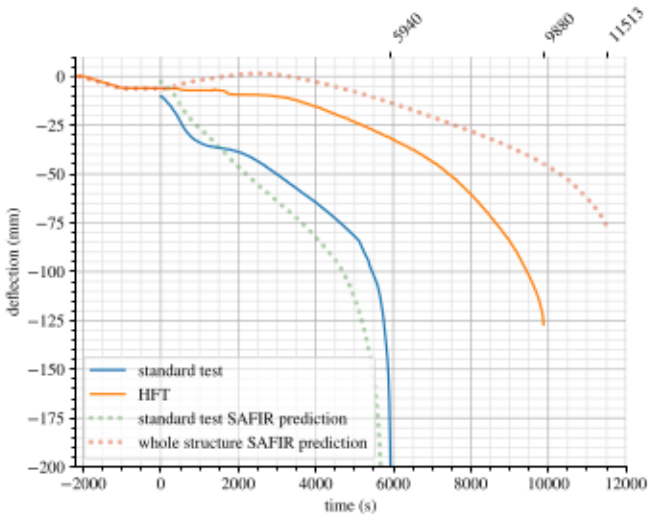

Fig. 17. Beam deflections.

the condition q_{prec} is almost never met. This precision degrades further from $t = 6000$ on θ_2, leading to a similar behaviour at a bigger scale. However, this mistake in the configuration of the controller only induced loss of precision and the system remained stable.

5.5. Discussion on the interest of a hybrid fire test

A standard fire test (*i.e.* non hybrid) of the same loaded beam has been performed on the same furnace [22]. The physical specimen was identical to the one discussed in this paper and casted at the same time. Being a standard test, the interaction between the tested element and the surrounding structure is assumed constant, with two constant moments applied at the beam extremities. No axial force is applied and the span loading is the same between both tests. During the standard test the spalling occurred much later than for the HFT, between 5100 and 5820 s of test. A comparison between the global beam deflections is made in Fig. 17. It can be noticed that the deflection increases quickly at the beginning of the standard test as the moments at the extremities are constants, unlike the HFT and the SAFIR simulation of the whole structure. The HFT beam deflection is also closer to the simulation than the standard test and hence *a priori* closer to reality. In the case of the standard test, failure of the element occur sooner, at 5950 s compared to 9880 s for the HFT, despite the fact that spalling occurred sooner in the case of HFT. The increased performance of the beam can be explained by different factors. The main one seems to be the failure modes that are very different as illustrated in Fig. 18. In the case of the standard test, the beam fails when a central plastic hinge appears whereas in the case of the HFT the efforts are redistributed to the surrounding structure and the failure occur only after the formation of a second plastic hinge near the left end of the beam quickly followed by the formation of the third one near the right end. Also, the horizontal restrain in the case of the HFT could increase the performance, acting like a 'post stressed' beam. The difference between the results of the HFT test and the SAFIR simulation may come from the spalling that was observed in the test, from the imperfections of the test mentioned in the previous section, and from the fact that the simulation is performed with generic thermal and mechanical properties and constitutive models (recommended in the Eurocodes) which may not correspond exactly to those of the material in place. The calculation is performed with the value of 47 MPa for the compressive strength of concrete, which is the mean value of the results from three cylinders.

6. Conclusion

In order to validate a new testing methodology, a full-scale, real time, three degree of freedom hybrid fire test has been performed. The control procedure and the adaptive controller exhibited good behaviour during the test, keeping the NS-PS system near the calculated equilibrium without any sign of instability, despite the occurrence of a large leap in one of the measured variables and the presence of measurement noise nearly 20 time larger than the one expected. A notable increase of the fire performance of the tested element is observed compared to a standard test and seems to be more consistent with the expected behaviour.

CRediT authorship contribution statement

Silvio Renard: Writing – original draft, Visualization, Software, Methodology, Investigation, Formal analysis, Data curation, Conceptualization. **Jean-Christophe Mindeguia:** Writing – review & editing, Validation, Supervision, Funding acquisition. **Fabienne Robert:** Writing – review & editing, Supervision, Resources, Project administration, Funding acquisition, Conceptualization. **Stéphane Morel:** Writing – review & editing, Supervision, Funding acquisition. **Jean-Marc Franssen:** Writing – review & editing, Supervision, Software, Resources, Methodology, Conceptualization.

Declaration of competing interest

The authors declare that they have no known competing financial interests or personal relationships that could have appeared to influence the work reported in this paper.

Data availability

Data will be made available on request.

Acknowledgements

This work was supported by a CIFRE convention n° 2017/0348 of the ANRT and the French Ministry of Higher Education, Research and Innovation. The modifications of SAFIR, used in the framework of the presented testing environment has been developed by Elke Mergny from Liege University, Belgium. The experimental setup and specimen have been widely inspired by the previous PhD work of Anna Sauca at the CERIB.

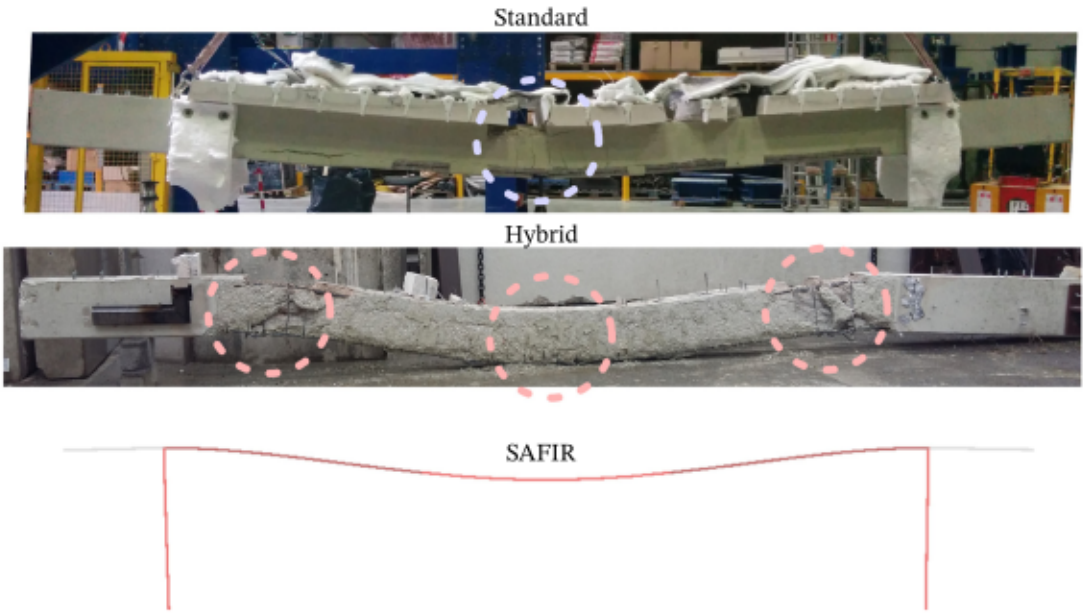

Fig. 18. Qualitative comparison of the irreversible deformations of the beam right after the standard test, a few days after the hybrid fire test and the deformations shortly before the failure in the SAFIR simulation of the whole structure. The circles indicate the positions of the plastic hinges that led to the failure.

References

[1] M. Korzen, G. Magonette, P. Buchet, Mechanical loading of columns in fire tests by means of the substructuring method, in: Interflam, 1999.

[2] M. Korzen, J.P. Rodrigues, L. Laím, Fire resistance tests on circular concrete columns, 2013.

[3] F. Robert, S. Rimlinger, C. Collignon, Structure Fire Resistance: a Joint Approach Between Modelling and Full Scale Testing (Substructuring System), FIB - Féd. Int. du Béton, 2010.

[4] H. Mostafaei, Hybrid fire testing for assessing performance of structures in fire—Application, Fire Saf. J. 56 (2013) 30–38, http://dx.doi.org/10.1016/j.firesaf.2012.12.003.

[5] H. Mostafaei, Hybrid fire testing for assessing performance of structures in fire—Methodology, Fire Saf. J. 58 (2013) 170–179, http://dx.doi.org/10.1016/j.firesaf.2013.02.005.

[6] J.M. Franssen, T. Gernay, Modeling structures in fire with SAFIR®: theoretical background and capabilities, J. Struct. Fire Eng. 8 (3) (2017) 300–323, http://dx.doi.org/10.1108/JSFE-07-2016-0010, Number: 3 Publisher: Emerald Publishing Limited.

[7] C.A. Whyte, K.R. Mackie, B. Stojadinovic, Hybrid simulation of thermomechanical structural response, J. Struct. Eng. 142 (2) (2016) 04015107, http://dx.doi.org/10.1061/(ASCE)ST.1943-541X.0001346, Number: 2 Publisher: American Society of Civil Engineers. URL https://ascelibrary.org/doi/abs/10.1061/%28ASCE%29ST.1943-541X.0001346.

[8] P. Schulthess, M. Neuenschwander, M. Knobloch, M. Fontana, Consolidated fire testing–a framework for thermomechanical modelling, in: COUPLED VI: Proceedings of the VI International Conference on Computational Methods for Coupled Problems in Science and Engineering, CIMNE, 2015, pp. 222–229.

[9] N. Tondini, G. Abbiati, L. Possidente, B. Stojadinovic, Hybrid simulation applied to fire testing: a newly conceived numerical framework, 2016.

[10] A. Sauca, T. Gernay, F. Robert, N. Tondini, J.-M. Franssen, Stability in Hybrid Fire Testing, in: 9th International Conference on Structures in Fire, SiF 16, Princeton University, NJ, USA, 2016.

[11] A. Sauca, E. Mergny, T. Gernay, J.M. Franssen, A method for hybrid fire testing: Development, implementation and numerical application, 2017, pp. 225–234, http://dx.doi.org/10.1201/9781315107202-26.

[12] R. Qureshi, N. Elhami-Khorasani, Instantaneous stiffness correction for hybrid fire testing, in: 10th International Conference on Structures in Fire, Belfast, 2018, pp. 933–940.

[13] E. Mergny, G. Drion, T. Gernay, J.M. Franssen, A PI-controller for hybrid fire testing in a non-linear environment, 2018.

[14] X. Wang, R.E. Kim, O.S. Kwon, I.H. Yeo, J.K. Ahn, Continuous real-time hybrid simulation method for structures subject to fire, J. Struct. Eng. 145 (12) (2019) 04019152, http://dx.doi.org/10.1061/(ASCE)ST.1943-541X.0002436, Number: 12 Publisher: American Society of Civil Engineers. URL https://ascelibrary.org/doi/abs/10.1061/%28ASCE%29ST.1943-541X.0002436.

[15] P. Schulthess, M. Neuenschwander, K.M. Mosalam, M. Knobloch, A computationally rigorous approach to hybrid fire testing, Comput. Struct. 238 (2020) 106301, http://dx.doi.org/10.1016/j.compstruc.2020.106301, Publisher: Pergamon URL http://www.sciencedirect.com/science/article/pii/S0045794920301048.

[16] E. Mergny, J.-M. Franssen, Real-time multi degrees of freedom hybrid fire testing, in: SiF 2020– the 11th International Conference on Structures in Fire, The University of Queensland, Brisbane, Australia, 2020.

[17] R. Qureshi, N. Elhami Khorasani, M. Sivaselvan, Developing real-time hybrid simulation to capture column buckling in a steel frame under fire, 2020, http://dx.doi.org/10.14264/384eb39.

[18] A. Sauca, N. Mortensen, A. Drustrup, G. Abbiati, Experimental validation of a hybrid fire testing framework based on dynamic relaxation, Fire Saf. J. 121 (2021) 103315, http://dx.doi.org/10.1016/j.firesaf.2021.103315, URL https://www.sciencedirect.com/science/article/pii/S0379711221000552.

[19] G. Abbiati, P. Covi, N. Tondini, O.S. Bursi, B. Stojadinović, A real-time hybrid fire simulation method based on dynamic relaxation and partitioned time integration, J. Eng. Mech. 146 (9) (2020) 04020104, http://dx.doi.org/10.1061/(ASCE)EM.1943-7889.0001826, Number: 9 Publisher: American Society of Civil Engineers URL https://ascelibrary.org/doi/abs/10.1061/%28ASCE%29EM.1943-7889.0001826.

[20] S. Renard, J.C. Mindeguia, F. Robert, S. Morel, J.M. Franssen, An adaptive controller for hybrid fire testing, Exp. Tech. 44 (6) (2020) 701–714, Publisher: Springer.

[21] Y. Shtessel, C. Edwards, L. Fridman, A. Levant, Sliding Mode Control and Observation, 2014, http://dx.doi.org/10.1007/978-0-8176-4893-0_6.

[22] A. Sauca, Development and Implementation of a Methodology for Hybrid Fire Testing Applied to Concrete Structures with Elastic Boundary Conditions (Ph.D. thesis), Université de Liège, Liège, Belgique, 2017.

[23] ISO 834-1 - Fire-resistance tests — Elements of building construction — Part 1: General requirements.

[24] S. Renard, Développement et implémentation d'un protocole automatique de conduite d'essais hybrides de résistance au feu (Ph.D. thesis), Université de Bordeaux, 2021, Issue: 2021BORD0137 URL https://tel.archives-ouvertes.fr/tel-03607733.

[25] EN 1992-1-2 - Eurocode 2: Design of concrete structures - Part 1-2: General rules - Structural fire design.

[26] EN 1991-1-2 - Eurocode 1: Actions on Structures Part 1-2 : General Actions – Actions on structures exposed to fire.